

The origin of MOND acceleration and deep MOND from acceleration fluctuation and energy cascade in dark matter flow

Zhijie (Jay) Xu,^{1*}

¹Physical and Computational Sciences Directorate, Pacific Northwest National Laboratory; Richland, WA 99352, USA

Accepted XXX. Received YYY; in original form ZZZ

ABSTRACT

MOND is an empirically motivated theory using modified gravity to reproduce many astronomical observations without invoking the dark matter hypothesis. Instead of falsifying the existence of dark matter, we propose that MOND is an effective theory naturally emerging from the long-range interaction and collisionless nature of dark matter flow. It describes the dynamics of baryonic mass suspended in fluctuating dark matter fluid. To maximize system entropy, the long-range interaction requires a broad size of halos to be formed. These halos facilitate an inverse mass and energy cascade from small to large mass scales with a constant rate of energy cascade $\varepsilon_u \approx -4.6 \times 10^{-7} m^2/s^3$. In addition to velocity fluctuation with a typical scale u , the long-range interaction leads to a fluctuation in acceleration with a typical scale a_0 . The velocity and acceleration fluctuations in dark matter flow satisfy $\varepsilon_u = -a_0 u / (3\pi)^2$ that determines a_0 , where factor 3π is from the angle of incidence. With $u_0 \equiv u(z=0) \approx 354.61 \text{ km/s}$ from N-body simulation, the value of $a_0 (z=0) \approx 1.2 \times 10^{-10} m/s^2$ can be easily obtained. While Planck constant \hbar , gravitational constant G , and ε_u are proposed to find the dark matter particle properties on the smallest scale, the velocity scale u , G , and ε_u determine the halo properties on the largest scale. For a given particle velocity v_p , maximum entropy distributions developed for dark matter flow lead to a particle kinetic energy $\varepsilon_k \propto v_p$ at small acceleration $a < a_0$ and $\varepsilon_k \propto v_p^2$ for $a > a_0$. Combining this with the constant rate of energy cascade ε_u , both Newtonian dynamics and "deep-MOND" behavior can be fully recovered. A notable (unexplained) coincidence of cosmological constant $\Lambda \propto (a_0/c)^2$ or a linear relation for light speed $c = (3\pi)^3 u_0$ might point to an entropic origin of dark energy from acceleration fluctuation with its density $\rho_{vac} \propto a_0^2/G$.

Key words: Dark matter; N-body simulations; MOND; Acceleration fluctuation; Energy cascade; Mass cascade

CONTENTS

- 1 Introduction
- 2 N-body simulations for dark matter flow
- 3 Energy cascade in dark matter flow
- 4 Maximum entropy distributions in dark matter flow
- 5 Fluctuation and distribution of acceleration in dark matter flow
- 6 The origin of MOND acceleration and deep-MOND behavior
- 7 Relevant scales in dark matter flow and connections with dark energy
- 8 Conclusions

1 INTRODUCTION

The most intriguing mystery of modern astrophysics is the dark matter problem, which originates from the discrepancy between required amount of mass by the astronomical observations and the directly observed amount of luminous mass. A striking example comes from the dynamical motions of astronomical objects. The flat rotation curves of spiral galaxies directly point to the discrepancy in mass: the total mass predicted from the Newtonian gravity is much greater than the observed luminous mass (Rubin & Ford 1970; Rubin et al. 1980).

The standard cosmological model (Λ CDM) interprets this mass discrepancy in terms of the cold dark matter (CDM). Though the

nature of dark matter is still unclear, it is widely believed that dark matter is cold (non-relativistic), collisionless, dissipationless (optically dark), non-baryonic, and barely interacting with baryonic matter except through gravity. In addition, dark matter (DM) must be sufficiently smooth on large scales with a fluid-like behavior. However, no conclusive signals have been detected in either direct or indirect searches of dark matter.

An alternative interpretation of the mass discrepancy resorts to the modification of our understanding of gravity that might eliminate the need of dark matter. The modified gravity must reproduce all astronomical observations (flat rotation curve etc.) with only the observed baryonic mass distribution. In 1977, Tully and Fisher established an empirical relation for rotation curves of galaxies with a wide range of masses M (Tully & Fisher 1977). In baryonic Tully-Fisher relation, the flat rotation velocity $v_f \propto M^{1/4}$ or $v_f^4 = GMa_0$ (McGaugh et al. 2000). Here G is the gravitational constant and a_0 is an empirical constant of acceleration. Similar scaling was also identified for the velocity dispersion σ for random motion of stars (Faber & Jackson 1976), i.e. $\sigma \propto M^{1/4}$.

The original modified Newtonian Dynamics (MOND) is a popular empirical model proposed to reproduce these astronomical observations without invoking the dark matter hypothesis (Milgrom 1983). Further developments were accomplished for the completeness of MOND. One example is the relativistic MOND (Sanders 1997; Bekenstein 2004). The basic idea of MOND is to introduce

* E-mail: zhijie.xu@pnnl.gov; zhijie.xu@hotmail.com

a critical scale of acceleration $a_0 \approx 1.2 \times 10^{-10} m/s^2$. The standard Newtonian mechanics $F = ma$ is recovered when acceleration $a \gg a_0$. While for "deep-MOND" regime with $a \ll a_0$, Newtonian mechanics should be modified to $F = ma^2/a_0$, i.e. the external force $F \propto a^2$. As an ad hoc empirically motivated theory, MOND successfully explains the shape of rotation curves (McGaugh & de Blok 1998), the baryonic Tully-Fisher relation (McGaugh et al. 2000; Lelli et al. 2019), and many other phenomena on galactic scale. This motivates the search of a fundamental origin of MOND paradigm.

In conventional wisdom, MOND is a competing empirical theory that potentially falsifies the dark matter hypothesis. In this paper, we propose that MOND can be an intrinsic feature of and consistent with the existence of dark matter. Instead of falsifying dark matter, MOND is an effective theory describing the dynamics of baryonic mass suspended in fluctuating dark matter fluid, which mimics the Brownian motion. The critical MOND acceleration is a natural result of acceleration fluctuation and energy cascade in the self-gravitating flow of dark matter. To explain this, we need to understand the nature of self-gravitating collisionless fluid dynamics (SG-CFD), a study for the motion of collisionless matter under its own gravity.

At first glance, both SG-CFD and regular hydrodynamic turbulence contain same features including the randomness, nonlinearity, and multiscale nature (see Xu 2022a, for a detailed comparison). The homogeneous isotropic incompressible turbulence has been widely studied for many decades (Taylor 1935, 1938; de Karman & Howarth 1938; Batchelor 1953). Turbulence consists of eddies (the building blocks of turbulence) that are interacting with each other. The classical picture of turbulence is an eddy-mediated cascade process (see Fig. 1) (see Xu 2021f, for more detail). Kinetic energy of large eddies feeds smaller eddies, which feeds even smaller eddies, and so on to the smallest scale η where viscous dissipation becomes dominant. There exists a range of scales with a scale-independent constant rate ε (unit: m^2/s^3) of energy passing down the cascade, i.e. the inertial range where the viscous force is negligible and inertial force is dominant (Fig. 1). This process (direct energy cascade) can be best described by a famous poem (Richardson 1922):

"Big whirls have little whirls, That feed on their velocity;
And little whirls have lesser whirls, And so on to viscosity."

While direct energy cascade is a dominant feature for 3D turbulence, there exists a range of scales over which kinetic energy is transferred from small to large length scales in 2D turbulence, i.e. an inverse energy cascade (Kraichnan 1967).

By comparing with hydrodynamic turbulence, the dark matter flow exhibits unique features due to its collisionless and long-range interaction nature (Xu 2022a, see slides for a good summary):

- (i) The long-range gravity requires a broad size of halos to be formed to maximize system entropy (Xu 2021c). Just like the Maxwell-Boltzmann distribution in kinetic theory of gases, maximum entropy distributions for velocity and energy can be analytically derived for SG-CFD and validated by N-body simulations (Xu 2021c). The linear scaling between particle energy and velocity at small acceleration can be essential to understand the "deep MOND" behavior (Eq. (5)).
- (ii) Halos are the building blocks of SG-CFD (counterpart to "eddies" in turbulence) and facilitate an inverse mass cascade from small to large mass scales that is absent in hydrodynamic turbulence (see Fig. 1). This leads to many new understandings of halo mass function and internal structure (density profiles etc.) in terms of the random-walk of halos in mass space (Xu 2021b,a).
- (iii) Both types of flow are non-equilibrium systems involving energy cascade across different scales (Xu 2021f). On system level,

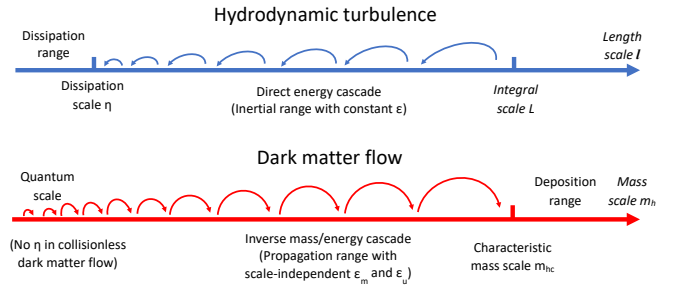


Figure 1. Schematic plot of the direct energy cascade in 3D hydrodynamic turbulence and the inverse mass/energy cascade in dark matter flow. Halos merge with free radicals (single mergers) to facilitate a continuous mass/energy cascade to large scales. Scale-independent mass flux ε_m and energy flux ε_u are expected for halos smaller than a characteristic mass (i.e. the propagation range corresponding to the inertial range for turbulence). Mass cascaded from small scales is consumed to grow halos at scales above the characteristic mass with a scale-dependent mass and energy flux (the deposition range that resembles the dissipation range in turbulence).

the mass/energy cascade is a key feature for intermediate statistically steady state of non-equilibrium systems to continuously maximize system entropy while evolving toward the limiting equilibrium (Xu 2021c). On halo level, entropy increases due to the energy transfer between random motion and mean flow in every individual halos (Xu 2022e). The baryonic-to-halo mass relation can be analytically derived from the energy cascade in dark matter flow (Xu 2022k).

(iv) In addition to the velocity fluctuation, the long-range interaction in dark matter flow also leads to fluctuations in acceleration that might explain the critical MOND acceleration a_0 . By contrast, in kinetic theory of gases, molecules undergo short-range elastic collisions with velocity fluctuation following a Maxwell-Boltzmann distribution to maximize system entropy. Acceleration fluctuation is not present in kinetic theory of gases.

(v) The viscous force is not present in collisionless dark matter flow. Without viscous force, there is no dissipation in SG-CFD and the smallest length scale of inertial range is not limited by viscosity (Fig. 1). This enables us to extend the scale-independent constant energy flux ε_u down to the smallest scales where quantum effects become important, and predict dark matter particle mass, size and other relevant properties (Xu 2022j).

(vi) Unlike hydrodynamic turbulence that is incompressible on all scales, dark matter flow exhibits scale-dependent flow behaviors, i.e. an incompressible flow for proper velocity (or constant divergence flow for peculiar velocity) on small scales and an irrotational flow on large scales (Xu 2022f,i,g). The two-thirds law for pairwise velocity dispersion holds for dark matter flow such that we can apply to identify dark matter particle properties (see Xu 2022j, Section 3).

In this paper, we first review some key properties of dark matter flow, followed by the origin of critical MOND acceleration and the "deep-MOND" behavior based on these properties.

2 N-BODY SIMULATIONS FOR DARK MATTER FLOW

The basic dynamics of dark matter flow is governed by the collisionless Boltzmann equations (CBE) (Mo et al. 2010) that can be numerically solved by particle-based N-body simulations (Peebles 1980). The simulation data for this work was generated from large scale N-body simulations by the Virgo consortium (Frenk et al. 2000;

Table 1. Numerical parameters of N-body simulation

Run	Ω_0	Λ	h	Γ	σ_8	L (Mpc/h)	N	m_p M_\odot/h	l_{soft} (Kpc/h)
SCDM1	1.0	0.0	0.5	0.5	0.51	239.5	256^3	2.27×10^{11}	36

Jenkins et al. 1998). The current work focuses on the matter-dominant simulations with $\Omega_0 = 1$ and cosmological constant $\Lambda = 0$. The same set of simulation data has been widely used in various studies such as the clustering statistics (Jenkins et al. 1998), the formation of halo clusters in large scale environments (Colberg et al. 1999), and testing models for halo abundance and mass functions (Sheth et al. 2001). Key parameters of N-body simulations are listed in Table 1, where h is the Hubble constant in the unit of $100 \text{ km}/(Mpc \cdot s)$, N is the number of particles, and m_p is the particle mass.

The friends-of-friends algorithm (FOF) was used to identify all halos in simulation that depends only on a dimensionless parameter b , which defines the linking length $b(N/V)^{-1/3}$, where V is the volume of simulation box. All halos in simulation were identified with a linking length parameter of $b = 0.2$ in this work. All halos identified were grouped into halo groups of different size according to halo mass m_h (or n_p , the number of particles in each halo), where $m_h = n_p m_p$. The total mass for a group of halos of mass m_h is $m_g = m_h n_h$, where n_h is the number of halos in that group. A halo-based non-projection approach is applied to perform the statistical analysis in this paper (Xu 2022i): i) all halos were identified with all particles divided into halo and out-of-halo particles; ii) instead of projecting particle field onto structured grid that involves information loss, a ‘‘pairwise’’ statistical analysis can be performed over all particle pairs with a given separation r . Simulation results are presented to describe the mass/energy cascade across halo groups of different mass scales.

3 ENERGY CASCADE IN DARK MATTER FLOW

The rate of energy cascade ε_u can be obtained from the formulation of mass/energy cascade (Xu 2021f,a). Alternatively, it can be derived from the energy evolution of entire collisionless system that can be described by a cosmic energy equation (Irvine 1961; Layzer 1963)(also see Xu 2022h, Section 3 for a different derivation),

$$\frac{\partial E_y}{\partial t} + H(2K_p + P_y) = 0. \quad (1)$$

This equation is a manifestation of energy conservation in expanding background. Here K_p is the specific (peculiar) kinetic energy, P_y is the specific potential energy in physical coordinate, $E_y = K_p + P_y$ is the total specific energy, and $H = \dot{a}/a$ is the Hubble parameter.

The cosmic energy equation (1) admits a power-law solution of $K_p \propto t$ and $P_y \propto t$ (see Fig. 2) such that a constant rate of energy production ε_u can be defined from the linear relation $K_p = -\varepsilon_u t$ and estimated as (Xu 2021f, 2022h)

$$\varepsilon_u = -\frac{K_p}{t} = -\frac{3}{2} \frac{u^2}{t} = -\frac{3}{2} \frac{u_0^2}{t_0} = -\frac{9}{4} H_0 u_0^2 \approx -4.6 \times 10^{-7} \frac{m^2}{s^3}, \quad (2)$$

where $u_0 \equiv u(t = t_0) \approx 354.61 \text{ km}/s$ is the one-dimensional velocity dispersion in dark matter flow from N-body simulation in Section 2.

The proportional constant ε_u has a profound physical meaning as the rate of energy cascade across different mass scales (Xu 2021f) that is facilitated by the inverse mass cascade (Xu 2021a). The negative value $\varepsilon_u < 0$ reflects the ‘‘inverse’’ energy cascade. The constant ε_u is a fundamental quantity that determines the critical MOND acceleration, i.e. $a_0 = (3\pi)^2 (-\varepsilon_u/u) \approx 1.2 \times 10^{-10} \text{ m}/s^2$ (see Eq.

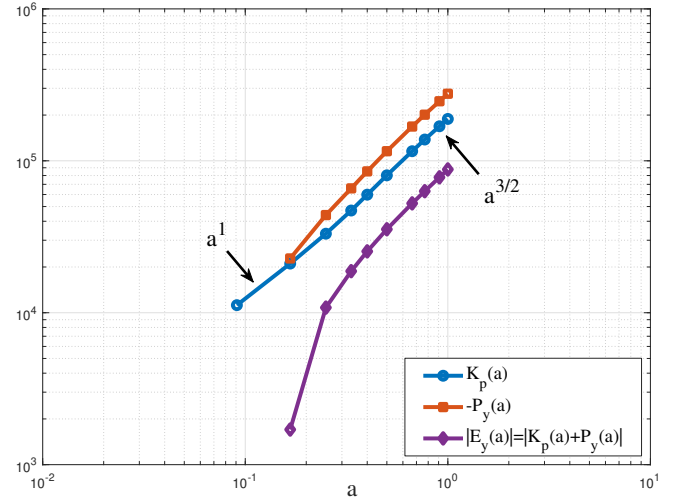


Figure 2. The time variation of specific kinetic and potential energies (km^2/s^2) from N-body simulation. Both energies exhibit power-law scaling with the scale factor a , i.e. $K_p(a) = -\varepsilon_u t \propto a^{3/2} \propto t$ and $P_y(a) \propto a^{3/2} \propto t$. The proportional constant ε_u is the rate of energy cascade that is estimated in Eq. (2).

(14)). In addition, for collisionless dark matter flow with gravity being the only interaction involved, the absence of viscosity enables us to extend the scale-independent energy cascade down to the smallest scale where quantum effects are dominant. Combining the energy flux ε_u , Planck constant \hbar , and gravitational constant G on the smallest scale, the mass of dark matter particles can be estimated to be around 10^{12} GeV with a size on the order of 10^{-13} m (Xu 2022j) (see Table 2 for other relevant properties).

4 MAXIMUM ENTROPY DISTRIBUTIONS IN DARK MATTER FLOW

The halo-mediated mass/energy cascade is an intermediate statistically steady state for non-equilibrium dark matter flow to continuously maximize system entropy while evolving towards the limiting equilibrium. In the kinetic theory of gases, the Boltzmann distribution is the maximum entropy distribution for velocity in equilibrium. In dark matter flow (SG-CFD), the maximum entropy distributions of DM particle velocity, speed, and energy are also gradually developed through continuous mass/energy cascade (Xu 2021c).

For system with long-range interaction and gravitational potential $V(r) \propto r^n$ ($-2 < n < 0$), a broad size of halos are required to be formed to maximize system entropy. Applying the virial equilibrium for mechanical equilibrium in halos and the maximum entropy principle for statistical equilibrium of global system, the maximum entropy distributions can be analytically derived. The halo mass function can be demonstrated as a direct result of entropy maximization (Xu 2021e). The maximum entropy distribution for velocity (the X distribution) involves a shape parameter α and a velocity scale v_0 (Xu 2021c),

$$X(v) = \frac{1}{2\alpha v_0} \frac{e^{-\sqrt{\alpha^2 + (v/v_0)^2}}}{K_1(\alpha)}, \quad (3)$$

where $K_y(x)$ is a modified Bessel function of *second kind*. Parameter α dominates the shape of X distribution. The X distribution approaches a double-sided Laplace (exponential) distribution with $\alpha \rightarrow 0$ and a Gaussian distribution with $\alpha \rightarrow \infty$, respectively. For

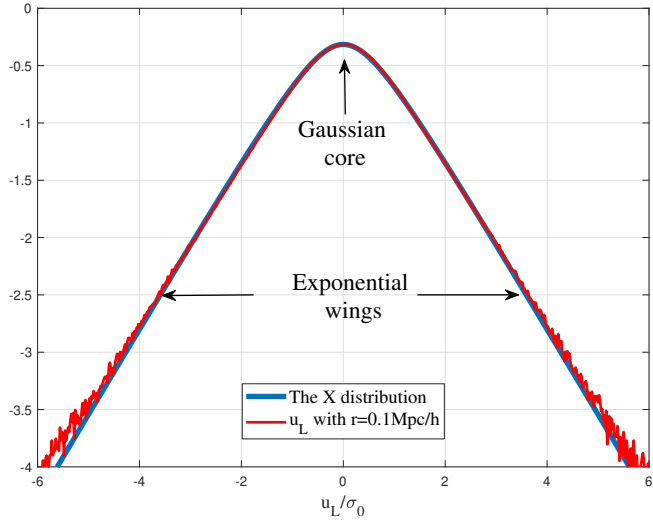


Figure 3. The X distribution with a unit variance compared with the velocity distribution from N -body simulation (u_L normalized by σ_0). Vertical axis is in the logarithmic scale (\log_{10}). The X distribution with $\alpha = 1.33$ and $v_0^2 = 1/3\sigma_0^2$ matches the velocity distribution on small scale r , where all pairs of particles are likely from the same halo. The Gaussian core ($u_L < v_0$) and exponential wings ($u_L > v_0$) can be clearly identified.

intermediate α , the X distribution naturally exhibits a Gaussian core at small velocity $v \ll v_0$ and exponential wings at large velocity $v \gg v_0$, as shown in Fig. 3.

In Fig. 3, the longitudinal velocity u_L is computed as the projection of particle velocity \mathbf{u} along the vector of separation \mathbf{r} for a pair of particles, i.e. $u_L = \mathbf{u} \cdot \mathbf{r}$. Particle velocity is normalized by σ_0^2 to have a unit variance. Here distribution parameters $\alpha = 1.33$, $v_0^2 = 1/3\sigma_0^2$, and $\sigma_0^2 = \text{var}(u_L)$ on the scale of $r \equiv |\mathbf{r}| = 0.1 \text{ Mpc}/h$. The scale and redshift dependence of velocity distributions in dark matter flow are also extensively studied with a halo-based non-projection approach (see Xu 2022i, Section 5), where the shape parameter $\alpha \equiv \alpha(z)$ can be redshift dependent. In this paper, the same approach is also applied to study the acceleration fluctuation and distribution.

Finally, the specific particle energy $\varepsilon(v)$ for dark matter particles with a given speed $v \equiv |\mathbf{v}|$ can be obtained from maximum entropy distributions (see Xu 2021c, Eq. (47) and Fig. 6),

$$\begin{aligned} \varepsilon(v) &= \varepsilon_P(v) + \varepsilon_K(v) = \frac{3}{2} \left(1 + \frac{2}{n}\right) v_0^2 \sqrt{\alpha^2 + \left(\frac{v}{v_0}\right)^2}, \\ \varepsilon_P(v) &= \frac{3}{n} v_0^2 \sqrt{\alpha^2 + \left(\frac{v}{v_0}\right)^2}, \quad \varepsilon_K(v) = \frac{3}{2} v_0^2 \sqrt{\alpha^2 + \left(\frac{v}{v_0}\right)^2}, \end{aligned} \quad (4)$$

where specific energy $\varepsilon(v)$ includes both kinetic ε_K and potential energy ε_P . Here $\varepsilon(v)$ follows a linear scaling for large velocity

$$\varepsilon(v) \approx \frac{3}{2} \left(1 + \frac{2}{n}\right) v_0 v \quad \text{for } v \gg v_0, \quad (5)$$

$$\varepsilon(v) \approx \frac{3}{2} \left(1 + \frac{2}{n}\right) \left(\alpha v_0^2 + \frac{v^2}{2\alpha}\right) \quad \text{for } v \ll v_0,$$

where n is the exponent of gravitational potential $\phi \propto r^{-n}$ with $n=-1$ for Newtonian gravity. The specific kinetic energy ε_K for particles with a given speed $v = |\mathbf{v}|$ should also follow $\varepsilon_K(v) \propto v^2$ for low-speed ($v \ll v_0$), which is the standard Newtonian behavior. However,

$\varepsilon_K(v) \propto v_0 v$ for high-speed particles ($v \gg v_0$) is a unique feature of dark matter flow.

Finally, let's see why kinetic energy can be proportional to particle velocity. High-speed particles are usually in the outer region of halos with extremely small acceleration. Their dynamics is much easier to be affected by the presence of external gravitational field (inter-halo gravitational force from all other halos) due to the long-range nature of gravity. The superimposition of all intra- and inter-halo interactions leads to the linear scaling $\varepsilon_K(v) \propto v$, which also emerges as a result of entropy maximization. This scaling can be demonstrated by N -body simulation (see Xu 2021c, Fig. 6) and is critical for understanding the "deep-MOND" behavior in Section 6. It might be also worth to explore any potential connection with external field effect in MOND (Milgrom 1986). By contrast, the dynamics of low-speed particles in halo core region is dominated by the intra-halo interaction only with a Newtonian behavior such that $\varepsilon_K(v) \propto v^2$.

5 FLUCTUATION AND DISTRIBUTION OF ACCELERATION IN DARK MATTER FLOW

The density and velocity distributions were extensively studied for dark matter flow (Xu 2022i). This section focus on the distribution of acceleration. In kinetic theory of gases, molecules undergo random elastic collisions with a short-range of interaction, where acceleration fluctuation is not present. By contrast, the long-range gravity in dark matter flow inevitably leads to fluctuations in particle acceleration, in addition to the fluctuation in velocity. This unique feature hints to the potential generalization of standard Brownian/Langevin dynamics to include acceleration fluctuation for dark matter flow. There can be many interesting work to explore along this direction.

In this section, the distribution of acceleration is explicitly studied to demonstrate that the critical MOND acceleration a_0 can be related to the fluctuation of acceleration. By computing the total force on each particle, the proper acceleration \mathbf{a}_p for particle i is

$$\mathbf{a}_p = \frac{Gm_p}{a^2} \sum_{j \neq i}^N \frac{\mathbf{x}_i - \mathbf{x}_j}{|\mathbf{x}_i - \mathbf{x}_j|^3}, \quad (6)$$

where \mathbf{x}_i and \mathbf{x}_j are the comoving spatial coordinates of particles i and j . Summation is running over all other particles except i . Periodic boundary is also taken care of in force calculation with a total of 26 repeats of simulation domain in three-dimension.

Figure 4 plots the redshift variation of acceleration distribution, i.e. the distribution of Cartesian component [a_{px}, a_{py}, a_{pz}] of acceleration vector \mathbf{a}_p for all particles. The particle acceleration evolves from an initial Gaussian distribution at high redshift to a distribution with a long tail $\propto a_p^{-3}$ for large acceleration in halo core region. Tail starts to form at around $z=5$ due to the formation of halos.

Just like the halo-based non-projection approach for velocity distributions (Xu 2022i), we identify all halos in N -body system and divide all DM particles into halo and out-of-halo particles since distributions are evolving differently for different types of particles.

Figure 5 plots the redshift evolution of distributions of a_{hp} for halo particles (solid lines) and a_{op} for out-of-halo particles (dash lines). The long tail $\propto a_{hp}^{-3}$ at large acceleration comes from halo core region with higher density. The maximum particle acceleration is determined by the highest density at halo core and seems independent of redshift. With inverse mass cascade (Xu 2021a), more particles are accreted into the halo outer region and the distribution gradually extends to smaller acceleration. The distribution of a_{op} for out-of-halo particles is relatively Gaussian for all redshifts. Acceleration

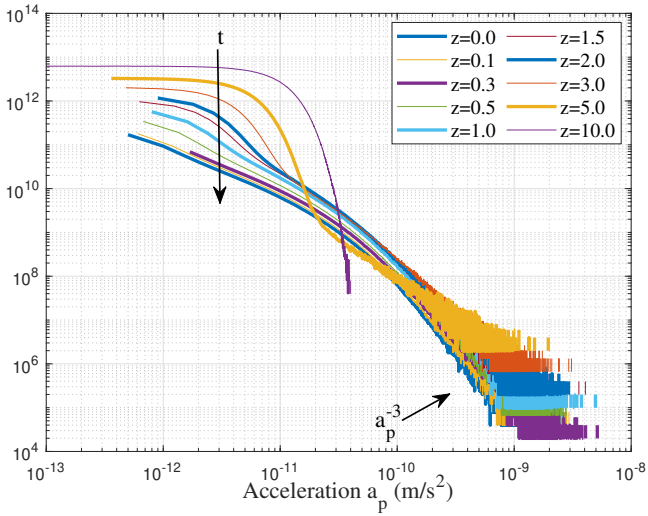


Figure 4. The redshift evolution of the distribution of particle acceleration a_p . A long tail $\propto a_p^{-3}$ is gradually formed from $z=5$ due to the formation of halo structures.

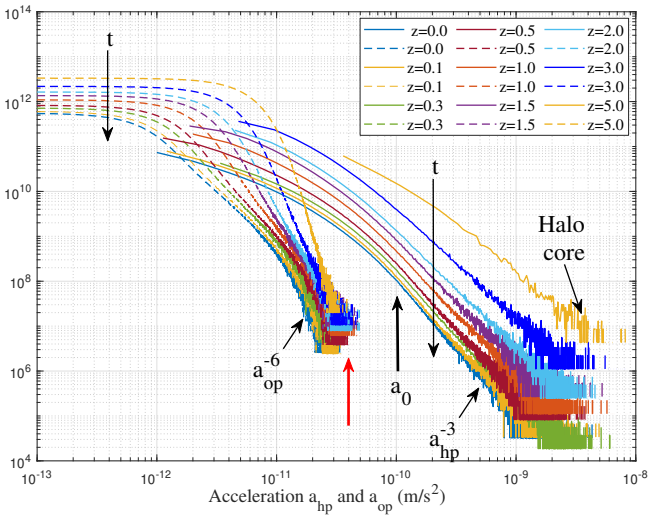


Figure 5. The redshift evolution of halo particle acceleration a_{hp} (solid lines) and out-of-halo particle acceleration a_{op} (dash lines). A long tail $\propto a_{hp}^{-3}$ at large acceleration is a typical feature from halo particles in core region. The distribution of a_{op} for out-of-halo particles is relatively Gaussian. For both types of particles, acceleration decreases with time (see Fig. 6). Critical MOND acceleration ($a_0 \approx 10^{-10} m/s^2$) is marked in the plot (black arrow).

decreases with time due to the expanding space (Fig. 6). The out-of-halo particles with the greatest acceleration should be those particles close to halos that they are going to merge with (red arrow). More study should be pursued on the theoretical models of acceleration distribution and correlation function of acceleration on all scales.

Figure 6 plots the time variation of typical accelerations ($\sqrt{3}$ ×standard deviation of distributions in Figs. 4 and 5, i.e. the root-mean-square acceleration) for all particles (blue), halo particles (black), out-of-halo particles (red), and halos (green), where the factor $\sqrt{3}$ is for the magnitude of acceleration vector in 3D space. The halo acceleration a_h is the mean acceleration of all particles in the same halo. All typical accelerations decrease with time (ap-

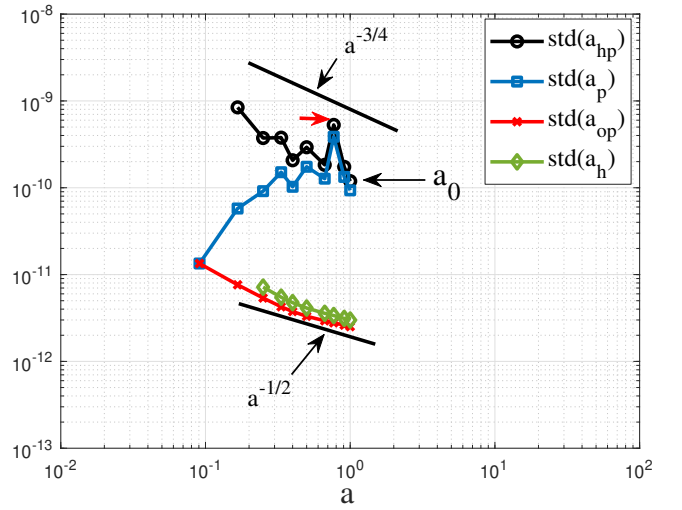


Figure 6. The variation of typical (root-mean-square) accelerations (m/s^2) with scale factor a for all particles (a_p : blue), halo particles (a_{hp} : black), out-of-halo particles (a_{op} : red), and halos (a_h : green), respectively. All accelerations decrease with time. At $z=0$, the typical acceleration of halo particles matches the critical MOND acceleration $a_0 = 1.2 \times 10^{-10} m/s^2$. The halo acceleration a_h matches the out-of-halo particle acceleration a_{op} and is much smaller ($\sim 10^{-12} m/s^2$) due to weaker gravity on large scale.

proximately $\propto a^{-3/4}$ for halo particles and $\propto a^{-1/2}$ for out-of-halo particles and halos). The only exception is the halo particle acceleration at $z=0.3$ (red arrow) that is greater than acceleration at both $z=0.5$ and $z=0.1$, which requires further confirmation from other N-body simulations. On large scale, halos and out-of-halo particles have similar accelerations that are much smaller than the acceleration of halo particles due to greater distance ($\sim 10^{-12} m/s^2$, green and red lines). At $z=0$, the typical acceleration of halo particles matches the critical MOND acceleration, where $a_0 = 1.2 \times 10^{-10} m/s^2$.

Similarly, Figure 7 plots the variation of velocity variance (kinetic energy) with scale factor a . The variance of halo velocity v_h matches the out-of-halo particle velocity v_{op} with a scaling $\propto a$. This is the scaling in the linear regime on large scale and consistent with the velocity correlation model (see Xu 2022f, Section 5.1). The variance of all particles (blue line) is dominated by out-of-halo particles at early time ($\langle v_p^2 \rangle \propto a$) and transition to $\langle v_p^2 \rangle \propto a^{3/2}$ at a later time (dominated by halo particle velocity).

Next, we identify all halos in N-body system and group halos according to their size n_p (the number of particles in halo) or halo mass $m_h = n_p m_p$. For every halo, the acceleration \mathbf{a}_{hp} and velocity \mathbf{v}_{hp} of halo particles can be decomposed into the contribution due to intra-halo interaction from all other particles in the same halo,

$$\mathbf{a}_{hp}^i = \mathbf{a}_{hp} - \langle \mathbf{a}_{hp} \rangle_h = \mathbf{a}_{hp} - \mathbf{a}_h \quad \text{and} \quad (7)$$

$$\mathbf{v}_{hp}^i = \mathbf{v}_{hp} - \langle \mathbf{v}_{hp} \rangle_h = \mathbf{v}_{hp} - \mathbf{v}_h,$$

and the contribution due to inter-halo interaction from all other particles in different halos (i.e. the halo acceleration and velocity),

$$\mathbf{a}_h = \langle \mathbf{a}_{hp} \rangle_h = \frac{1}{n_p} \sum_{k=1}^{n_p} \mathbf{a}_{hp}, \quad \mathbf{v}_h = \langle \mathbf{v}_{hp} \rangle_h = \frac{1}{n_p} \sum_{k=1}^{n_p} \mathbf{v}_{hp}, \quad (8)$$

where $\langle \cdot \rangle_h$ stands for average of a quantity over all particles in a given halo. On halo level, the typical acceleration in each halo a_h^i can be

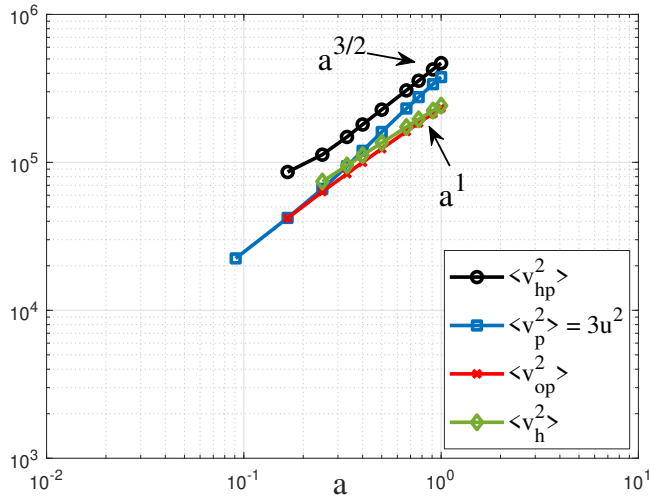


Figure 7. The variation of velocity dispersion (km^2/s^2) with scale factor a for all particles (v_p : blue), halo particles (v_{hp} : black), out-of-halo particles (v_{op} : red), and halos (v_h : green), respectively. All velocity dispersion increase with time. The dispersion of halo velocity v_h matches the out-of-halo particle velocity v_{op} with a scaling $\propto a$. The dispersion of all particles velocity (blue) is dominated by out-of-halo particles at early time ($\langle v_p^2 \rangle \propto a$) and by halo particle at a later time $\langle v_p^2 \rangle \propto a^{3/2}$.

computed as the root-mean-square of intra-halo particle acceleration \mathbf{a}_{hp}^i for all particles in the same halo, i.e. $a_h^i = \langle |\mathbf{a}_{hp}^i|^2 \rangle_h^{1/2}$. The halo acceleration \mathbf{a}_h is the mean acceleration of all particles in the same halo, i.e. $\mathbf{a}_h = \langle \mathbf{a}_{hp} \rangle_h$ in Eq. (8).

On group level (a group of all halos with the same size n_p), the typical acceleration in halo (a_{hg}^i) can be computed as the mean intra-halo acceleration a_h^i for all halos in the same group, i.e. $a_{hg}^i = \langle a_h^i \rangle_g$, where $\langle \cdot \rangle_g$ stands for the average over all halos in the same group. The typical halo acceleration a_{hg} can be computed as the root-mean-square of halo acceleration \mathbf{a}_h for all halos in the same group, i.e. $a_{hg} = \langle |\mathbf{a}_h|^2 \rangle_g^{1/2}$. Similar statistics were also applied to particle velocity \mathbf{v}_{hp} to obtain the halo virial dispersion σ_v^2 and halo velocity dispersion σ_h^2 (see Xu 2021f, Section 4.1).

Figure 8 plots the variation of typical accelerations in halos (a_{hg}^i : solid lines) and acceleration of halos (a_{hg} : dash lines) with halo size n_p at different redshifts z . Halo mass $m_h = n_p m_p$ with $m_p = 2.27 \times 10^{11} M_\odot/h$ (Table 1). For same halo size n_p , both accelerations decrease with time. Acceleration in halos a_{hg}^i increases with halo size and reaches about $10^{-10} m/s^2$ for large halos. Acceleration of halos a_{hg} is relatively independent of halo size, much smaller than acceleration in halos and roughly on the order of $10^{-12} m/s^2$ due to weaker gravity between halos on large scale.

6 THE ORIGIN OF MOND ACCELERATION AND DEEP-MOND BEHAVIOR

Note that the typical acceleration in halos (a_{hp} in Fig. 6) at $z=0$ matches the critical MOND acceleration $a_0 = 1.2 \times 10^{-10} m/s^2$ (Milgrom 1983), which hints a_0 might be an intrinsic property of dark matter flow due to the fluctuation of acceleration. The value of a_0 is still empirical and phenomenological without a good theory. A potential theory for critical acceleration a_0 can be made here based

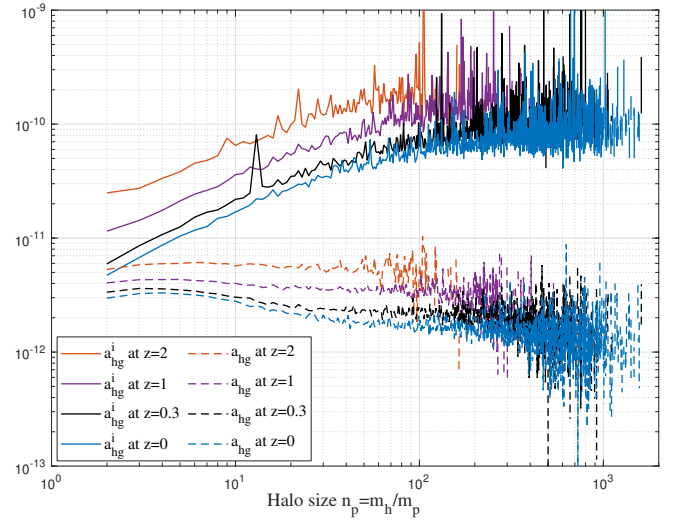


Figure 8. The variation of typical acceleration (m/s^2) in halos (a_{hg}^i : solid lines) and acceleration of halos (a_{hg} : dash lines) with halo size n_p at different redshifts z . Halo mass $m_h = n_p m_p$. Both accelerations decrease with time at a given halo size, while acceleration in halos increases with halo size (roughly $a_{hg}^i \propto (m_h)^{2/3} a^{-1}$ for small n_p and $a_{hg}^i \propto (m_h)^{1/6} a^{-1}$ for large n_p) and reaches about $10^{-10} m/s^2$ for large halos. Acceleration of halos a_{hg} is independent of halo size n_p , much smaller and on the order of $10^{-12} m/s^2$.

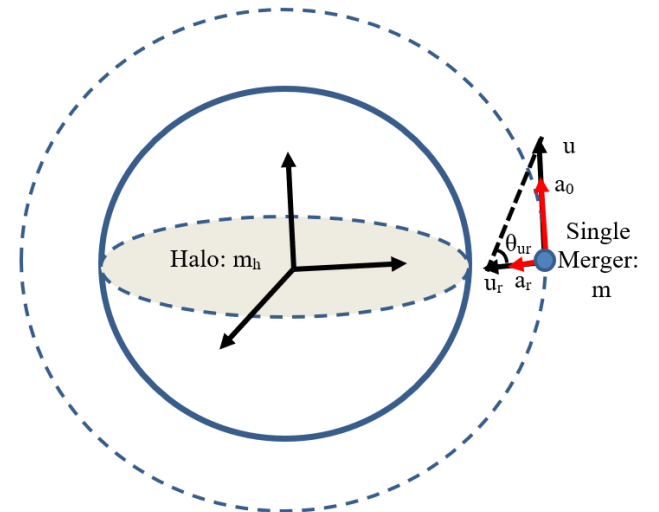


Figure 9. The schematic plot for inverse mass/energy cascade from a single merging between halo and single mergers. For an infinitesimal interval dt , that process should only involve the merging of a halo (mass: m_h) with a single merger (mass: m). The single merger has a typical velocity u (a) (black) and acceleration a_0 (a) (red). Dash line is the boundary of that halo. The angle of incidence satisfies $\cot(\theta_{ur}) = 1/(3\pi)$.

on the inverse mass/energy cascade and acceleration fluctuation in dark matter flow (Xu 2021a,f).

In a finite time interval Δt , the hierarchical structure merging might involve multiple substructures merging into a single large structure. For an infinitesimal time interval dt , that process should involve the merging of two and only two substructures (see Fig. 9) such that the two-body collapse is the most elementary process for halo mass

accretion and inverse mass cascade. This elementary process can be described by a two-body collapse model (TBCM) (Xu 2021d). The continuous elementary merging between a halo and a single merger facilitates the inverse mass and energy cascade (Xu 2021a,f).

Let's consider a two-body merging, where a single merger has a mass m , a typical velocity $u(a)$ from velocity fluctuation, and a typical acceleration $a_0(a)$ from acceleration fluctuation, right before the merging with a halo of mass m_h (see Fig. 9). The velocity and acceleration of single merger are likely aligned on large scale in the linear regime, i.e. \mathbf{u} and \mathbf{a}_0 point to the same direction (Zeldovich 1970). Due to the gravitational interaction with halo to be merged, the single merger right on the boundary (dash line) has a relative motion toward the center of halo $u_r = u \cot(\theta_{ur})$ (the radial velocity) and a radial acceleration with $a_r = a_0 \cot(\theta_{ur})$. The angle of incident θ_{ur} can be related to the critical value β_{s2} for an equilibrium two-body collapse (see Xu 2021d, Eq. (104)),

$$\cot(\theta_{ur}) = \frac{u_r}{v_{cir}} = \beta_{s2} = \frac{1}{3\pi}, \quad (9)$$

where v_{cir} is the circular velocity at the surface of halo ($u \approx v_{cir}$). Here β_{s2} is a constant that is related to the critical halo density as $\Delta_c = 2/(\beta_{s2})^2 = 18\pi^2$ (see Xu 2021d, Eq. (89)). This is also true for isothermal halos where the ratio between circular velocity and radial flow is $v_{cir}/u_r = 3\pi$ (see Xu 2021b, Eq. (31)).

The angle of incidence can also be easily demonstrated with the radial velocity $u_r = Hr_h = v_{cir}/(3\pi)$ for virialized halos from stable clustering hypothesis (SCH), where r_h is halo size. Here we can write the halo mass as

$$m_h = \frac{4}{3}\pi r_h^3 \Delta_c \bar{\rho} \Rightarrow v_{cir} = \frac{Gm_h}{r_h} = Hr_h \sqrt{\frac{\Delta_c}{2}} = 3\pi u_r, \quad (10)$$

where Hubble parameter $H = 8\pi G \bar{\rho}/3$ and $\bar{\rho}(t)$ is the mean background matter density.

Now let's compute the constant rate of energy cascade in dark matter flow in several different ways. That rate (ϵ_u in m^2/s^3) represents the energy flux/transfer across halos of different mass scales. In the first approach, it can be determined by the change of total kinetic energy of all halo particles due to the intra-halo motion (defined in Eqs. (7) and (8)), i.e. a dot product between \mathbf{a}_{hp}^i and \mathbf{v}_{hp}^i ($\mathbf{a} = d\mathbf{v}/dt$),

$$\epsilon_u = - \left\langle \mathbf{a}_{hp}^i \cdot \mathbf{v}_{hp}^i \right\rangle = - \langle \mathbf{a}_{hp} \cdot \mathbf{v}_{hp} \rangle + \underbrace{\langle \mathbf{a}_h \cdot \mathbf{v}_h \rangle}_1, \quad (11)$$

where \mathbf{a}_{hp} and \mathbf{v}_{hp} are halo particle total acceleration and velocity, while \mathbf{a}_{hp}^i and \mathbf{v}_{hp}^i are particle acceleration and velocity relative to the motion of halos (due to intra-halo interaction). The average is taken over all halo particles in all halos. Terms \mathbf{a}_h and \mathbf{v}_h are the acceleration and velocity of halos, i.e. the mean acceleration and velocity of all particles in a given halo (Eq. (8)). The change of kinetic energy due to the motion of halos (term 1 in Eq. (11)) does not contribute to energy cascade and should be excluded.

In the second approach, the inverse mass/energy cascade is facilitated by a series of merging with single mergers (Xu 2021a,f). The rate of kinetic energy cascade might be directly determined from a typical merging process, i.e. a two-body merging in Fig. 9. During each merging, the kinetic energy transferred from small to large mass scale (from m_h to $m_h + m$) comes from the change of kinetic energy of that single merger at the instant of merging, mostly via the relative motion along radial direction (Fig. 9). The motion in tangential direction does not contribute to the energy cascade (no relative motion along tangential direction). For a single merger with a typical velocity $u(a)$ and a typical acceleration $a_0(a)$, the rate of energy transfer

ϵ_u approximately reads

$$\epsilon_u = -a_r u_r = -a_0(a) \cot(\theta_{ur}) u(a) \cot(\theta_{ur}), \quad (12)$$

where $\epsilon_u < 0$ for inverse cascade. This expression resembles the first expression in Eq. (11), but is obtained from the elementary two-body merging process. This picture also reveals that the energy cascade in dark matter flow is enabled by the mass cascade. By contrast, energy cascade in turbulence (Fig. 1) is facilitated by the deformation of vortex, i.e. a vortex stretching mechanism (see Xu 2021f, for details).

In the third approach, by considering the energy evolution in entire N-body system, the rate of energy cascade is approximately the change of specific kinetic energy for entire system, or rate of energy production in kinetic energy. It is a constant of time (see Fig. 2 and Eq. (2)) and should read

$$\epsilon_u \approx -\frac{3}{2} \frac{u^2}{t} = -\frac{3}{2} \frac{u_0^2}{t_0} = -\frac{9}{4} H_0 u_0^2 = -4.6 \times 10^{-7} \frac{m^2}{s^3}. \quad (13)$$

All three approaches should give the same rate of energy cascade. Combining Eqs. (9)-(13) together, the typical acceleration $a_0(a)$ can be related to the rate of energy cascade ϵ_u as

$$a_0(a) = -\frac{\Delta_c}{2} \cdot \frac{\epsilon_u}{u} = -(3\pi)^2 \frac{\epsilon_u}{u} = \frac{81}{4} \pi^2 H_0 \frac{u_0^2}{u} \propto a^{-3/4}, \quad (14)$$

where with $u_0 = 354.61 \text{ km/s}$ and $H_0 = 100 h \text{ km}/(\text{s} \cdot \text{Mpc}) \approx 1.62 \times 10^{-18} 1/\text{s}$ (with $h = 0.5$),

$$a_0(a=1) \approx 200 H_0 u_0 \approx 1.2 \times 10^{-10} \text{ m/s}^2. \quad (15)$$

The redshift dependence of critical acceleration $a_0(a) \propto a^{-3/4} = (1+z)^{3/4}$ seems consistent with literature that a_0 decreases with scale factor a , but at a slower rate than $a_0(a) \propto a^{-3/2}$ (Dai & Lu 2017; Milgrom 2017).

Finally, we demonstrate that the critical MOND acceleration a_0 can be fully determined by ϵ_u (Eq. (14)). Just like the peculiar velocity, there exists a fluctuation of acceleration in dark matter flow. The critical MOND acceleration originates from the typical scale of acceleration fluctuation, i.e. the MOND theory might be an intrinsic property of and fully consistent with the theory of fluctuating dark matter flow. In this regard, instead of falsifying, the MOND theory might indeed support the existence of dark matter.

More insights can be briefly outlined here for the origin of so-called "deep-MOND" behavior, where the external force $F \propto a^2$ when particle acceleration is much smaller than the fluctuation of acceleration ($a_p \ll a_0$). To simplify the calculation, let's assume a one-dimensional self-gravitating collisionless dark matter fluid with a typical velocity scale v_0 and an acceleration scale a_0 due to the fluctuations of velocity and acceleration. A baryonic particle with mass m_p , velocity v_p , and acceleration $a_p = dv_p/dt$, moves through the collisionless fluid under external force F_p . The driving force F_p can be of any nature including gravity. This is an exact analogue of the Brownian motion with moving particles suspended in a viscous liquid. Let's assume the baryonic mass is in equilibrium with dark matter fluid such that both "phases" share the same rate of energy cascade ϵ_u . To respect the nature of dark matter flow we discussed, the velocity dispersion v_p^2 of that baryonic particle should increase linearly with time (Eq. (13)) with a proportional constant $\epsilon_u = -a_0 v_0$ (θ_{ur} in Eq. (12) does not present for 1D system),

$$\frac{1}{2} \frac{dv_p^2}{dt} = v_p \frac{dv_p}{dt} = a_p v_p = a_0 v_0 = -\epsilon_u. \quad (16)$$

The external force F_p can be computed from the change of specific kinetic energy,

$$F_p v_p = m_p \frac{d\epsilon_K}{dt}. \quad (17)$$

For "deep-MOND" regime where $a_p \ll a_0$ or $v_p \gg v_0$ (outer region of halos), the specific kinetic energy of baryonic mass $\varepsilon_K(v) \propto v_0 v_p$ (same as dark matter particles from Eq. (5)) as both "phases" are in equilibrium). Force in "deep-MOND" can be obtained from Eqs. (16) and (17) such that the external force $F_p \propto m_p a_p^2$, i.e.

$$F_p \propto m_p \frac{v_0}{v_p} a_p = m_p \frac{a_p^2}{a_0}. \quad (18)$$

On the other hand, for particles with low speed or high acceleration, i.e. $a_p \gg a_0$ or $v_p \ll v_0$ in the core region of halos, the specific kinetic energy $\varepsilon_K(v) \propto v_p^2$ such that the standard Newton's law $F_p \propto m_p a_p$ can be fully recovered from Eq. (17).

There are two key ingredients necessary for this simplistic view of MOND: i) the constant rate of energy cascade for dark matter flow (Eq. (16)); and ii) the kinetic energy proportional to particle speed for low acceleration (Eq. (5)). If both a_0 and v_0 are the standard deviation of acceleration and velocity fluctuation, Eq. (16) represents a new "uncertainty" principle in dark matter flow, such that the more precisely velocity is determined, the less precisely its acceleration can be determined, and vice versa. Future work is required to further refine and develop this simple idea.

7 RELEVANT SCALES IN DARK MATTER FLOW AND CONNECTIONS WITH DARK ENERGY

In hydrodynamic turbulence, the viscous dissipation is the only mechanism to dissipate the kinetic energy and destroy enstrophy in turbulence. There exists a limiting length scale $\eta = (v^3/\varepsilon)^{1/4}$ in Fig. 1 (Kolmogorov scale) that is determined by both rate of energy dissipation ε and the molecular viscosity ν . However, that scale is not present in collisionless dark matter flow. Without a viscous force, there is no dissipation range in dark matter flow and the smallest length scale of inertial range is not limited by viscosity.

This unique feature enables us to extend the scale-independent constant energy flux ε_u down to the smallest scale, where quantum effects become important, if there are no other known interactions or forces involved except gravity. Assuming gravity is the only interaction between dark matter particles (traditionally denoted by X), the dominant physical constants on the smallest scale are the (reduced) Planck constant \hbar , the gravitational constant G , and the rate of energy cascade ε_u . All other relevant quantities including the dark matter particle mass and size can be easily found by a simple dimensional analysis and listed in Table 2 (also see Xu 2022j, for details).

Now let's focus on the other end of the propagation range. This is the largest scale with a scale-independent constant rate of energy cascade in Fig. 1, beyond which energy cascade becomes scale-dependent (Xu 2021f). On that scale, the dominant physical constants are the gravitational constant G , the rate of energy cascade ε_u , the velocity scale $u_0 = 354.61 \text{ km/s}$, and the scale factor a . Universe expansion is only important on large scale and should not play a role on the smallest scale where structure is well bounded. Any quantity Q on the largest scale can be written as $Q \propto G^x \varepsilon_u^y u_0^z a^P$.

Similarly, all relevant quantities associated with the typical halo on that scale are also obtained and listed in Table 2. The length scale r_s should be the size of halos with a critical mass m_{hc} . It should be related to the length scale r_t defined by the crossover between transverse velocity correlation and longitudinal velocity correlation (see Xu 2022f, Fig. 4). Below r_s , flow is of constant divergence nature and pair of particles on that scale is more likely from the same halo. Above r_s , flow is irrotational and pair of particles on that scale is more likely from different halos. The density scale $\rho_c \approx \Delta_c \bar{\rho}$ is the

Quantity	Small scale	Large scale $z = 0$
Length	$l_X = (-2G\hbar/\varepsilon_u)^{1/3}$ $= 3.12 \times 10^{-13} \text{ m}$	$r_s = -u_0^3/\varepsilon_u$ $= 1.57 \text{ Mpc/h}$ (see Xu 2022i, Eq. (57))
Time	$t_X = (-32G^2\hbar^2/\varepsilon_u^5)^{1/9}$ $= 7.51 \times 10^{-7} \text{ s}$	$t_c = (-u_0^2/\varepsilon_u)$ $= 8.67 \times 10^9 \text{ year}$
Mass	$m_X = (-256\varepsilon_u\hbar^5/G^4)^{1/9}$ $= 0.90 \times 10^{12} \text{ GeV}$ (see Xu 2022j, Eq. (19))	$m_{hc} = -u_0^5/(G\varepsilon_u)$ $= 0.9 \times 10^{14} M_\odot$ (see Xu 2022k, Eq. (28))
Velocity	$v_X = (\varepsilon_u^2\hbar G/4)^{1/9}$ $= 4.16 \times 10^{-7} \text{ m/s}$	$v_c = u_0$ $= 354.61 \text{ km/s}$
Acceleration	$a_X = (-4\varepsilon_u^7/(\hbar G))^1/9$ $= 1.11 \text{ m/s}^2$	$a_0 = -(3\pi)^2 \varepsilon_u/u_0$ $= 1.2 \times 10^{-10} \text{ m/s}^2$ (see Eq. (14))
Energy	$E_X = (-\hbar^7 \varepsilon_u^5/(32G^2))^1/9$ $= 0.87 \times 10^{-9} \text{ eV}$	$E_c = -u_0^7/(G\varepsilon_u)$ $= 2.3 \times 10^{55} \text{ J}$
Density	$\rho_X = (\varepsilon_u^{10}/(2\hbar^4 G^{13}))^1/9$ $= 5.33 \times 10^{22} \text{ kg/m}^3$	$\rho_c = \varepsilon_u^2/(Gu_0^4)$ $= 2.0 \times 10^{-25} \text{ kg/m}^3$
Energy density (pressure)	$\rho_{eX} = (16\varepsilon_u^{14}/(\hbar^2 G^{11}))^1/9$ $= 1.84 \times 10^{10} \text{ J/m}^3$	$\rho_{ec} = \varepsilon_u^2/(Gu_0^2)$ $= 2.52 \times 10^{-14} \text{ J/m}^3$
Diffusivity (viscosity)	$\nu_X = (-2\hbar^4 G^4/\varepsilon_u)^1/9$ $= 1.3 \times 10^{-19} \text{ m}^2/\text{s}$	$\nu_c = u_0^4/\varepsilon_u$ $= -3.39 \times 10^{28} \text{ m}^2/\text{s}$ (see Xu 2022g, Eq. (97))

Table 2. Relevant physical quantities on both small and large scale

average halo density, where $\bar{\rho} \approx 2 \times 10^{-27} \text{ kg/m}^3$ is the background matter density at $z = 0$.

The energy density or the pressure of halos on that scale is comparable with the CMB (cosmic microwave background) density $\rho_{CMB} \approx 4 \times 10^{-14} \text{ J/m}^3$, i.e. halo pressure on that scale is comparable with the background pressure from CMB. Both CMB and dark matter interact with baryonic masses with all three "phases" in some equilibrium on that scale. Finally, the "effective" viscosity on large scale (negative sign due to inverse mass cascade) is discussed in the statistical theory for dark matter flow (Xu 2022g).

The energy density ρ_{ec} might also set the scale for dark energy. With c being the speed of light, Λ being the cosmological constant, a coincidence was pointed out by Milgram (Milgram 2001) such that

$$a_0(z=0) \approx cH_0/(2\pi) \approx c(\Lambda/3)^{1/2}/(2\pi). \quad (19)$$

The rate of energy cascade ε_u can be related to c and Λ (Eq. (14))

$$\varepsilon_u \approx -\frac{u_0 c H_0}{2\pi(3\pi)^2} \approx -\frac{u_0 c (\Lambda/3)^{1/2}}{2\pi(3\pi)^2}, \quad (20)$$

and

$$\Lambda \approx 3(2\pi)^2(3\pi)^4 \left(\frac{\varepsilon_u}{u_0 c}\right)^2 = \frac{3(2\pi)^2}{c^2} a_0^2 \approx 2 \times 10^{-35} \frac{1}{s^2}. \quad (21)$$

Therefore, the dark energy density can be related to the fluctuation of acceleration as (also see energy density scale ρ_{ec} in Table 2)

$$\rho_{vac} = \frac{\Lambda c^2}{8\pi G} = \frac{(3\pi)^5}{2G} \left(\frac{\varepsilon_u}{u_0}\right)^2 = \frac{3\pi}{2} \frac{a_0^2 H_0}{GH} \approx 10^{-9} \text{ J/m}^3. \quad (22)$$

Instead of this coincidence, a more general thinking can be proposed for a linear relation between dispersion u_0 and light speed c with a proportional constant $\beta_c \approx (3\pi)^3$. With Eqs. (13) and (14),

$$c = \beta_c u_0 \Rightarrow a_0(z=0) = \frac{81\pi^2}{4\beta_c} H_0 c, \quad (23)$$

and similarly we have

$$\Lambda \approx \frac{(4\beta_c)^2 a_0^2 H_0}{27(3\pi)^4 c^2 H}, \quad (24)$$

$$\rho_{vac} = \frac{\Lambda c^2}{8\pi G} = \frac{2\beta_c^2}{9(3\pi)^5} \frac{a_0^2 H_0}{GH} \approx 4.5 \times 10^{-10} J/m^3.$$

The exact meaning of coincidence in Eq. (19) is not clear. Good understanding of coincidence in Eq. (23), i.e. $c \approx (3\pi)^3 u_0$, is also elusive. The factor 3π seems provide a connection between velocities in space of different dimensions (see Fig. 9 and Eq. (9) for velocity in 3D space projected onto the radial direction as the 1D radial flow). Any exotic ideas of dark matter in extra dimension that are able to explain this should be interesting.

Equation (22) or (24) might indicate some hidden relations between dark energy and velocity/acceleration fluctuations in dark matter flow ($\rho_{vac} \propto a_0^2$, i.e. the dark energy density is proportional to the acceleration fluctuation with a entropic origin). New ideas along this line might be worth to explore.

8 CONCLUSIONS

The main focus of this paper is the study of unique features of self-gravitating collisionless dark matter flow (SG-CFD) and the origin of MOND acceleration and "deep-MOND" behavior. In dark matter flow, the long-range interaction requires a broad size of halos to be formed to maximize system entropy. Halos facilitate an inverse mass and energy cascade from small to large mass scales with a constant rate of energy cascade $\varepsilon_u \approx -4.6 \times 10^{-7} m^2/s^3$.

The mass/energy cascade represents an intermediate statistically steady state of dark matter flow. In addition to the velocity fluctuation with a typical scale u , the long-range interaction of dark matter flow also leads to fluctuations in acceleration with a typical scale a_0 . In N-body simulation, the root-mean-square acceleration decreases with time and matches the critical MOND acceleration of $1.2 \times 10^{-10} m/s^2$ (Fig. 6). The maximum entropy distributions reveal particle energy proportional to velocity when particle acceleration is small (Eq. (5)).

Velocity and acceleration fluctuations in dark matter flow satisfy the relation $\varepsilon_u = -a_0 u / (3\pi)^2$ which gives $a_0 \approx 1.2 \times 10^{-10} m/s^2$. MOND might be an effective theory describing the dynamics of baryonic masses suspended in fluctuating dark matter fluid. Both Newtonian and "deep MOND" behavior can be recovered in this description. For mass propagation range in Fig. 1, relevant physical quantities on the smallest scale are determined by constants \hbar , G , and ε_u . The same quantities on the largest scale are determined by G , ε_u , $u_0 = 354.61 km/s$, and scale factor a (see Table 2).

Future study can be the potential generalization of Brownian/Langevin dynamics to consider the acceleration fluctuation for dark matter flow. More study should also be explored on the theoretical models for distributions of acceleration and any potential theory for connections between dark energy and the velocity and acceleration fluctuations in dark matter flow.

DATA AVAILABILITY

Two datasets underlying this article, i.e. a halo-based and correlation-based statistics of dark matter flow, are available on Zenodo (Xu 2022b,c), along with the accompanying presentation slides "A comparative study of dark matter flow & hydrodynamic turbulence and its applications" (Xu 2022a). All data files are also available on GitHub (Xu 2022d).

REFERENCES

- Batchelor G. K., 1953, *The Theory of Homogeneous Turbulence*. Cambridge University Press, Cambridge, UK
- Bekenstein J. D., 2004, *Physical Review D*, 70
- Colberg J. M., White S. D. M., Jenkins A., Pearce F. R., 1999, *Monthly Notices of the Royal Astronomical Society*, 308, 593
- Dai D. C., Lu C. Y., 2017, *Physical Review D*, 96
- Faber S. M., Jackson R. E., 1976, *Astrophysical Journal*, 204, 668
- Frenk C. S., et al., 2000, [arXiv:astro-ph/0007362v1](https://arxiv.org/abs/astro-ph/0007362v1)
- Irvine W. M., 1961, Thesis, HARVARD UNIVERSITY
- Jenkins A., et al., 1998, *Astrophysical Journal*, 499, 20
- Kraichnan R. H., 1967, *Physics of Fluids*, 10, 1417
- Layzer D., 1963, *Astrophysical Journal*, 138, 174
- Lelli F., McGaugh S. S., Schombert J. M., Desmond H., Katz H., 2019, *Monthly Notices of the Royal Astronomical Society*, 484, 3267
- McGaugh S. S., de Blok W. J. G., 1998, *Astrophysical Journal*, 499, 41
- McGaugh S. S., Schombert J. M., Bothun G. D., de Blok W. J. G., 2000, *Astrophysical Journal*, 533, L99
- Milgrom M., 1983, *Astrophysical Journal*, 270, 365
- Milgrom M., 1986, *ApJ*, 302, 617
- Milgrom M., 2001, *Acta Physica Polonica B*, 32, 3613
- Milgrom M., 2017, [arXiv:1703.06110](https://arxiv.org/abs/1703.06110)
- Mo H., van den Bosch F., White S., 2010, *Galaxy formation and evolution*. Cambridge University Press, Cambridge
- Peebles P. J. E., 1980, *The Large-Scale Structure of the Universe*. Princeton University Press, Princeton, NJ
- Richardson L. F., 1922, *Weather Prediction by Numerical Process*. Cambridge University Press, Cambridge, UK
- Rubin V. C., Ford W. K., 1970, *Astrophysical Journal*, 159, 379
- Rubin V. C., Ford W. K., Thonnard N., 1980, *Astrophysical Journal*, 238, 471
- Sanders R. H., 1997, *Astrophysical Journal*, 480, 492
- Sheth R. K., Mo H. J., Tormen G., 2001, *Monthly Notices of the Royal Astronomical Society*, 323, 1
- Taylor G. I., 1935, *Proceedings of the royal society A*, 151, 421
- Taylor G. I., 1938, *Proceedings of the Royal Society of London Series a-Mathematical and Physical Sciences*, 164, 0015
- Tully R. B., Fisher J. R., 1977, *Astronomy & Astrophysics*, 54, 661
- Xu Z., 2021a, [arXiv e-prints](https://arxiv.org/abs/2109.09985), p. [arXiv:2109.09985](https://arxiv.org/abs/2109.09985)
- Xu Z., 2021b, [arXiv e-prints](https://arxiv.org/abs/2109.12244), p. [arXiv:2109.12244](https://arxiv.org/abs/2109.12244)
- Xu Z., 2021c, [arXiv e-prints](https://arxiv.org/abs/2110.03126), p. [arXiv:2110.03126](https://arxiv.org/abs/2110.03126)
- Xu Z., 2021d, [arXiv e-prints](https://arxiv.org/abs/2110.05784), p. [arXiv:2110.05784](https://arxiv.org/abs/2110.05784)
- Xu Z., 2021e, [arXiv e-prints](https://arxiv.org/abs/2110.09676), p. [arXiv:2110.09676](https://arxiv.org/abs/2110.09676)
- Xu Z., 2021f, [arXiv e-prints](https://arxiv.org/abs/2110.13885), p. [arXiv:2110.13885](https://arxiv.org/abs/2110.13885)
- Xu Z., 2022a, A comparative study of dark matter flow & hydrodynamic turbulence and its applications, [doi:10.5281/zenodo.6569901](https://doi.org/10.5281/zenodo.6569901), <http://dx.doi.org/10.5281/zenodo.6569901>
- Xu Z., 2022d, Dark matter flow dataset, [doi:10.5281/zenodo.6586212](https://doi.org/10.5281/zenodo.6586212), https://github.com/ZhijieXu2022/dark_matter_flow_dataset
- Xu Z., 2022b, Dark matter flow dataset Part I: Halo-based statistics from cosmological N-body simulation, [doi:10.5281/zenodo.6541230](https://doi.org/10.5281/zenodo.6541230), <http://dx.doi.org/10.5281/zenodo.6541230>
- Xu Z., 2022c, Dark matter flow dataset Part II: Correlation-based statistics from cosmological N-body simulation, [doi:10.5281/zenodo.6569898](https://doi.org/10.5281/zenodo.6569898), <http://dx.doi.org/10.5281/zenodo.6569898>
- Xu Z., 2022e, [arXiv e-prints](https://arxiv.org/abs/2201.12665), p. [arXiv:2201.12665](https://arxiv.org/abs/2201.12665)
- Xu Z., 2022f, [arXiv e-prints](https://arxiv.org/abs/2202.00910), p. [arXiv:2202.00910](https://arxiv.org/abs/2202.00910)
- Xu Z., 2022g, [arXiv e-prints](https://arxiv.org/abs/2202.02991), p. [arXiv:2202.02991](https://arxiv.org/abs/2202.02991)
- Xu Z., 2022h, [arXiv e-prints](https://arxiv.org/abs/2202.04054), p. [arXiv:2202.04054](https://arxiv.org/abs/2202.04054)
- Xu Z., 2022i, [arXiv e-prints](https://arxiv.org/abs/2202.06515), p. [arXiv:2202.06515](https://arxiv.org/abs/2202.06515)
- Xu Z., 2022j, [arXiv e-prints](https://arxiv.org/abs/2202.07240), p. [arXiv:2202.07240](https://arxiv.org/abs/2202.07240)
- Xu Z., 2022k, [arXiv e-prints](https://arxiv.org/abs/2203.06899), p. [arXiv:2203.06899](https://arxiv.org/abs/2203.06899)
- Zeldovich Y. B., 1970, *Astronomy & Astrophysics*, 5, 84
- de Karman T., Howarth L., 1938, *Proceedings of the Royal Society of London Series a-Mathematical and Physical Sciences*, 164, 0192